

# **JGR** Atmospheres

## **RESEARCH ARTICLE**

10.1029/2020JD033381

#### **Key Points:**

- Characteristics and evolution of mesospheric gravity waves generated by the thunderstorm
- Momentum flux estimates were obtained on timescales of minutes
- Momentum flux values were found to be much larger than for typical mesospheric gravity waves

#### Correspondence to:

S. M. Smith, smsm@bu.edu

#### Citation:

Smith, S. M., Setvák, M., Beletsky, Y., Baumgardner, J., & Mendillo, M. (2020). Mesospheric gravity wave momentum flux associated with a large thunderstorm complex. *Journal of Geophysical Research: Atmospheres*, 125, e2020JD033381. https://doi.org/10.1029/2020JD033381

Received 1 JUL 2020 Accepted 5 OCT 2020 Accepted article online 8 OCT 2020

#### **Author Contributions:**

Conceptualization: Steven M. Smith Data curation: Steven M. Smith, Martin Setvák, Yuri Beletsky Formal analysis: Steven M. Smith Funding acquisition: Steven M. Smith, Martin Setvák Investigation: Steven M. Smith Methodology: Steven M. Smith

Smith
Resources: Steven M. Smith
Software: Steven M. Smith
Supervision: Steven M. Smith
Validation: Steven M. Smith
Visualization: Steven M. Smith

Project administration: Steven M.

Writing - original draft: Steven M.

Writing – review & editing: Steven M. Smith, Martin Setvák, Yuri Beletsky, Jeffrey Baumgardner, Michael Mendillo

©2020. American Geophysical Union. All Rights Reserved.

# Mesospheric Gravity Wave Momentum Flux Associated With a Large Thunderstorm Complex

Steven M. Smith<sup>1</sup>, Martin Setvák<sup>2</sup>, Yuri Beletsky<sup>3</sup>, Jeffrey Baumgardner<sup>1</sup>, and Michael Mendillo<sup>1</sup>

<sup>1</sup>Center for Space Physics, Boston University, Boston, MA, USA, <sup>2</sup>Satellite Department, Czech Hydrometeorological Institute, Prague, Czech Republic, <sup>3</sup>Las Campanas Observatory, La Serena, Chile

**Abstract** We report on estimates of the vertical flux of horizontal momentum associated with an extensive and bright mesospheric gravity wave event that occurred over the El Leoncito Observatory, Argentina (31.8°S, 69.3°W), during the night of 17–18 March 2016. Using a combination of ground-based and space-based data sources, we propose that the event was generated by a large and distant thunderstorm complex located to the southeast of the observation site. The nightglow, including the wave structures, was easily visible to naked eye observers, a phenomenon known as a Bright Night. Such "extreme events" illuminate the important role of upward coupling in space weather research.

**Plain Language Summary** In this paper, we report on a large and extensive gravity wave event that occurred in the upper mesosphere, 90 km over the El Leoncito Observatory, Argentina (31.8°S, 69.3°W), during the night of 17–18 March 2016. The wave event was clearly visible to the naked eye—an event known as a Bright Night. Using a combination of ground-based and satellite data sources, we present evidence that the wave event was generated by a large thunderstorm complex located several hundred kilometers away from El Leoncito. We estimated the amount of momentum flux associated with the waves was over an order of magnitude larger than typically observed. Events such as these illustrate that large amounts of wave energy and momentum can be transported from thunderstorms and other weather-related events, up into the space environment near 100 km. They also illuminate the important role of upward coupling in space weather research.

#### 1. Introduction

Several past studies have shown that significant amounts of wave momentum and energy are transported from the lower levels of the atmosphere up to the stratosphere (Dewan et al., 1998; Picard et al., 1998; Wu, 2004; Wu & Eckermann, 2008; Wu & Jiang, 2002). The association of mesospheric gravity waves with troposphere disturbances, such as thunderstorm centers, has also been reported previously on several occasions (e.g., Sentman et al., 2003; Taylor et al., 1987; Taylor & Hapgood, 1988; Vadas et al., 2009, 2012; Xu et al., 2015, 2019; Yue et al., 2009, 2013, 2014). Here we report on a mesospheric wave event of remarkable brightness, spatial extent, and longevity that appears to originate from a large thunderstorm complex. The event was bright enough to be visible to the naked eye by one of the coauthors (Y. B.). Figure 1 is a color photograph taken by the coauthor during the event from the Las Campanas Observatory in Chile, which is located over the Andes range approximately 335 km northwest of El Leoncito Observatory.

The wave event occurred during a night of enhanced mesospheric nightglow emission, known as a Bright Night (Armstrong, 1982; Barnard, 1911; Bates, 1960; Gledhill, 1874; Herse, 1988; Hoffmeister, 1951, 1952, 1960; Peterson, 1979; Rayleigh, 1931; Skey, 1902; Shepherd & Cho, 2017; Smith et al., 2003; Taylor et al., 1987, 1995). Bright Nights are nights that exhibit marked enhancement (approximately tenfold) in the nightglow emissions. The cause is still uncertain. One study suggests that they be the result of large-scale dynamics (Shepherd & Cho, 2017). There have been numerous reports of "striped" or "ribboned" skies during Bright Nights (Barnard, 1911; Hoffmeister, 1951, 1952, 1960; Skey, 1902)—probable examples of mesospheric gravity wave activity occurring during such periods with the enhanced nightglow providing a backdrop for the waves to be visible, such as the present case.

Although reports of the occurrence of bright nights visually have decreased in recent years—indubitably due to the increasing use of anthropogenic lighting throughout the world—the number of bright nightglow

SMITH ET AL. 1 of 12



**Figure 1.** Color image of naked-eye airglow and gravity waves from the Las Campanas Observatory, Chile, taken by one of the coauthors (Y. B.) during the wave event on 18 March 2016. The panoramic image is a stitched composite of 12 images, each with an exposure time of 30 s.

observations in the last decade, from astrophotographers using improvedperformance full-frame cameras, has increased greatly.

Utilizing a multidiagnostic suite of ground-based measurements and four satellite data sets, we present observations and analysis of a large and bright mesospheric gravity wave event generated by a thunderstorm complex. We also present high time resolution wave momentum flux measurements of the event during the course of the night with a view to quantifying and understanding the contribution that thunderstorms and similar tropospheric disturbances may make via upward coupling processes to the mesosphere and higher regions.

The precise role of gravity waves in the variability of the mesosphere and lower thermosphere is still not well known. Small-scale short-period gravity waves, that is, those typically recorded by all-sky imagers (ASIs), are known to transport considerable amounts of wave momentum into the region and, as a result, contribute significantly to its dynamics and variability.

It is becoming clear that upward coupling events such as the one reported here contribute significant amounts of wave momentum and energy into the upper atmosphere and thus are an important component in the dynamics of space weather.

#### 2. All-Sky Instrumentation and Data

The Boston University (BU) ASI ( $180^{\circ}$ ) at the El Leoncito Observatory ( $31.8^{\circ}$ S,  $69.3^{\circ}$ W) comprises an Andor back-illuminated, bare  $2048 \times 2048$ -pixel CCD camera (Baumgardner et al., 1993; Martinis et al., 2006, 2017; Smith et al., 2006, 2009, 2015) equipped with a 16-mm fish-eye lens.

The OH, Na, O(<sup>1</sup>S) all-sky images were reduced via our standard procedure; bias and dark subtraction, flat fielding to remove vignetting by the optical system, van Rhijn brightening, and atmospheric extinction (see Baumgardner et al., 2007, for a more comprehensive description). The images then underwent a star removal procedure and were calibrated into Rayleigh brightness units using a calibrated standard light source.

The images were also mapped onto the Earth's surface using known star positions and the nominal or measured altitudes of each emission layer—a process known as unwarping. The OH layer altitude (87.9 km) was obtained from measurements made during the SABER overpass (see below). For the other two emissions, heights of Na ~90 km, O(¹S) ~97 km was used.

Vertical cross sections of the wave field were derived from the individual images along the direction of wave propagation through zenith, using a width of 21 pixels (~10 km). The horizontal wavelengths and phase speeds of the gravity waves were derived via cross-correlation analysis of the unwarped OH and O( $^1$ S) image cross sections. Estimates of the vertical flux of horizontal momentum (per unit mass) associated with the gravity waves were derived from the image data using the method devised by Swenson and Liu (1998) and Vargas et al. (2007).

#### 3. Observations

#### 3.1. El Leoncito All-Sky Images

#### 3.1.1. Mesospheric Activity

A mesospheric gravity wave event was recorded by the BU ASI in three mesospheric nightglow emissions—OH (broadband IR, 695–1,050 nm), Na (589.3 nm), and O( $^1$ S) (557.7 nm)—over El Leoncito during the night of 18 March 2016 UT. The wave event was characterized by an expansive train of gravity waves propagating toward northwest at an azimuth of 305° and exhibiting noticeable wavefront curvature.

All-sky imaging observations began at 00:00 UT and ended at 09:42 UT, a total observation period of 9 hr 42 min. Cloud cover hindered the observations during the period of 00:00–2:30 UT, but glimpses through the clouds indicated that the event continued during that period and that its lifetime extended beyond the

SMITH ET AL. 2 of 12

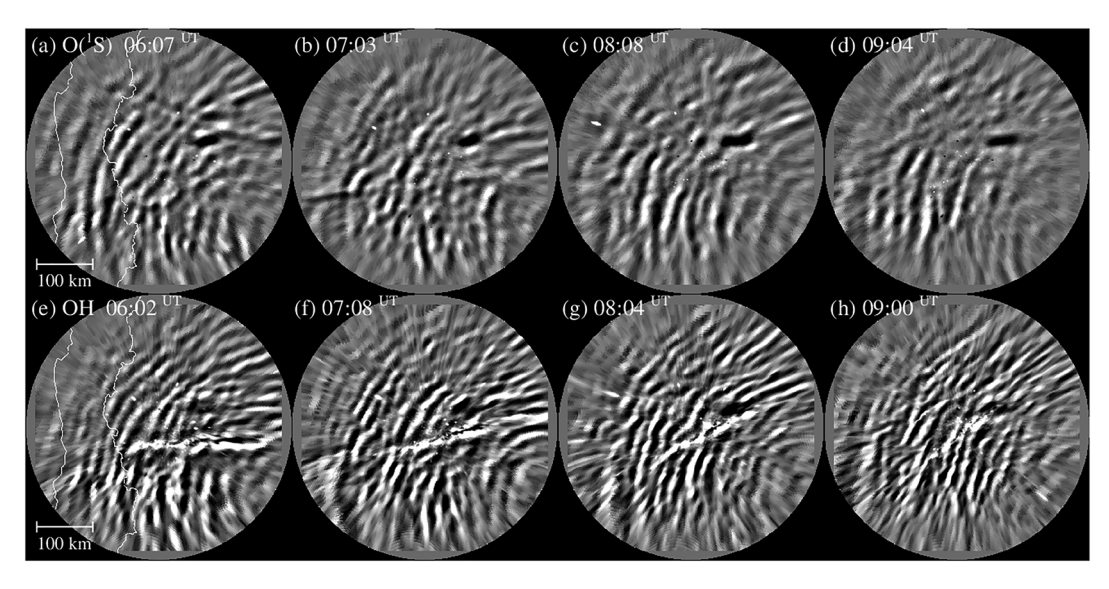


**Figure 2.** All-sky images in the mesospheric emissions  $O(^1S)$  (a–d) and OH (e–h) showing the morphologies and time history of the gravity wave event at hourly intervals at the El Leoncito Observatory on 18 March 2016.

total observing period. Determinations of zenith airglow brightness and wave amplitude were obtained during 06:00–10:00 UT, when the moon had set and the sky was cloud free.

Figure 2 shows the morphology and time history of the gravity wave event in the  $O(^1S)$  (top panels) and OH (bottom panels) emissions during the night. The wavefronts are markedly curved, which suggests that the source region was local or regional. Furthermore, the similar morphology, orientation, propagation speed, and scale sizes in the three mesospheric emissions suggested a common origin for the wave event.

The curved morphology of the wavefronts was similar to mesospheric gravity wave events reported previously and shown to be associated with a convective thunderstorm system (e.g., Sentman et al., 2003; Yue et al., 2013, 2009). The center of curvature associated with the wavefronts was determined by fitting points to the concentric wave patterns in the images for the period 05:00–9:40 UT. Each individual curved wavefront yielded a locus representing the center of curvature, which was assumed to be the epicenter for the origin of that wavefront.

The direction and range of the apparent wave epicenter(s) coincided with the general location of a large and active thunderstorm complex that was located to the southeast of El Leoncito. Different regions of convective activity occurred as the system moved eastward and evolved during the course of the night. Consequently, the apparent origin of the waves increased in distance from El Leoncito, from  $300 \pm 35$  km at 05:00 UT to  $610 \pm 40$  km at 09:00 UT, evidently as the thunderstorm evolved as it evolved eastward during the night.

A comparison of the phase patterns associated with the waves in the OH, Na, and O( $^1$ S) emissions indicated a downward phase progression and, hence, an upward propagation of wave energy. The gravity waves exhibited a mean horizontal phase speed of  $c_{\rm obsOH} = 39.9~{\rm m~s^{-1}}~(\sigma = 8.3~{\rm m~s^{-1}})$  and  $c_{\rm obsO(^1S)} = 38.6~{\rm m~s^{-1}}$  ( $\sigma = 5.1~{\rm m~s^{-1}}$ ), which is typical for mesospheric gravity waves. The phase speeds remained constant throughout the night, within the uncertainties. The mean horizontal wavelengths were  $\lambda_{\rm xOH} = 35.1~{\rm km}$  ( $\sigma = 5.4~{\rm km}$ ) and  $\lambda_{\rm xO(^1S)} = 42.8~{\rm km}~(\sigma = 5.1~{\rm km})$ . The observed wave period  $\tau$  was determined by  $\tau = \lambda_{\rm x}/c_{\rm obs}$ , which yielded  $\tau_{\rm OH} = 14.7 \pm 0.6~{\rm min}$  and  $\tau_{\rm O(^1S)} = 18.5 \pm 0.7~{\rm min}$ . The OH waves exhibited smaller horizontal scale sizes compared to those in the O( $^1$ S) emission. This is also evident in Figure 2 and suggested that the wave was refracted or Doppler-shifted before reaching the altitude of the O( $^1$ S) emission.

For short-period waves, the linear dispersion equation yields  $\tan \varphi = \lambda_z/\lambda_x = [(\tau/\tau_b)^2 - 1]^{-1/2}$ , where  $\varphi$  is the propagation angle of the wave relative to the horizontal direction and  $\tau_b$  is the Brunt-Vaisala period (~4–5 min, determined from the SABER profiles). Using this relation,  $\varphi_{\rm OH} = 16.5^{\circ} \pm 1.2^{\circ}$  to the

SMITH ET AL. 3 of 12



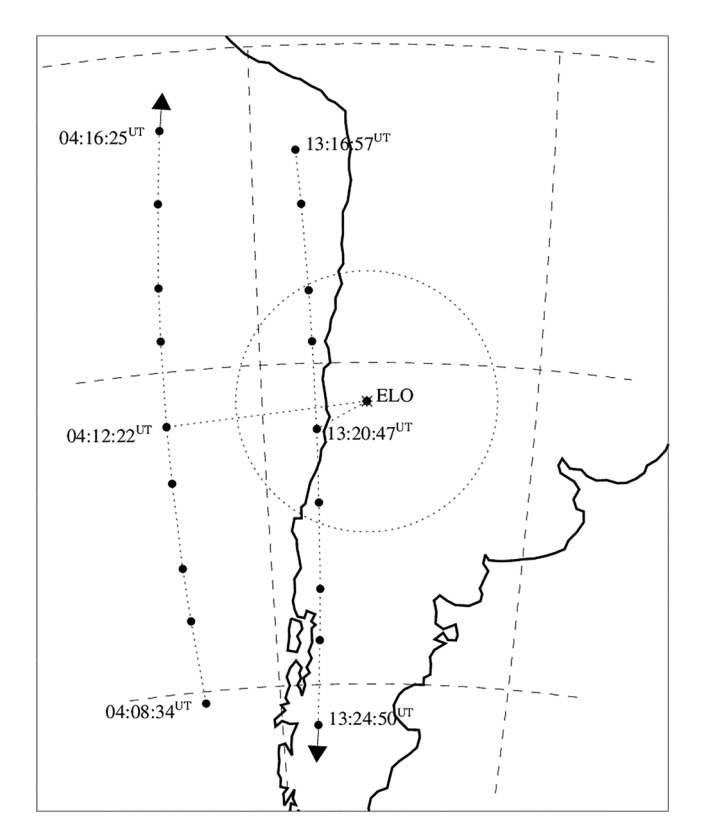


**Figure 3.** Location map of the El Leoncito Observatory showing the ground tracks during the TIMED SABER overpasses of 04:12 and 13:20 UT on 18 March 2016. The dotted black circle represents the all-sky imager's field of view at  $5^{\circ}$  elevation angle at  $96 \text{ km } (\text{O(}^{1}\text{S)})$ .

horizontal and  $\lambda_{\text{zOH}} = 10.4 \pm 0.9$  km. Similarly, for the O( $^{1}$ S) emission,  $\varphi_{\text{O(S)}} = 16.1^{\circ} \pm 1.8^{\circ}$  and  $\lambda_{\text{zO(S)}} = 12.4 \pm 1.5$  km. Although the values for  $\lambda_{z}$  here are not derived from the intrinsic wave period or the intrinsic phase speed, they are consistent with the value of  $\lambda_{z}$  derived from the SABER temperature profiles using FFT analysis (see below).

The travel time of the gravity waves from the thunderstorm to the upper mesosphere can be determined by using the vertical group velocity  $c_{gz}$ , where  $c_{gz} = (\lambda_z/\tau)\cos^2\varphi$ , which yields  $c_{gz} = 10.8 \pm 2.2$  m s<sup>-1</sup>. If we assume that the waves originated from an altitude near 15 km, the travel time to the OH layer at 88 km is  $114 \pm 23$  min.

The mean zenith OH brightness measured by the BU ASI during 6:00–10:00 UT was 7.1 kR ( $\sigma$  = 2.1 kR), and 695 R ( $\sigma$  = 104 R) for the O( $^1$ S) emission. Both are consistent with previous bright night occurrences (e.g., Smith et al., 2003). The mean-to-peak wave brightness amplitudes, as absolute and percentage values, were OH = 660 R (10.3%) and O( $^1$ S) = 42 R (6.1%), which are comparable with previous events, such as Smith et al. (2003). The Smith et al. (2003) case comprised a bore disturbance, which is a trapped mode of propagation and known to exhibit nonlinear amplitude growth, whereas the present event was consistent with an upward propagating gravity wave.

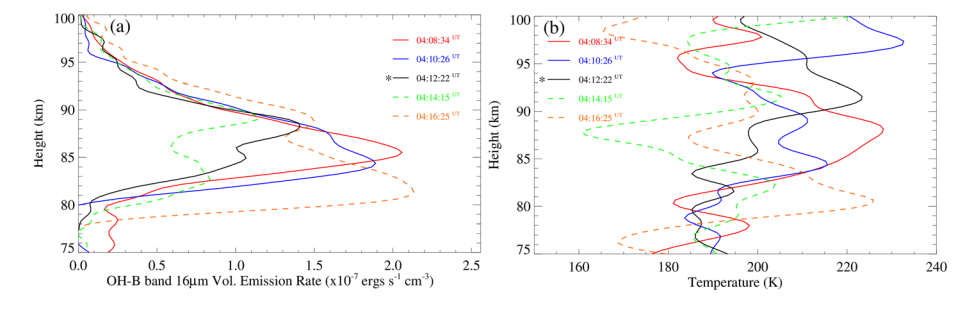
In addition to the mesospheric emissions, the BU ASI also records the thermospheric  $O(^{1}D)$  630.0-nm emission, which originates from near 250 km in altitude, near the peak of the F region ionosphere. An analysis of the 630.0-nm imagery revealed no evidence of gravity wave activity in the thermosphere arising from the mesospheric activity.

#### 3.2. TIMED SABER Observations

The National Aeronautics and Space Administration (NASA) TIMED satellite overflew El Leoncito twice on 18 March 2016 and the onboard

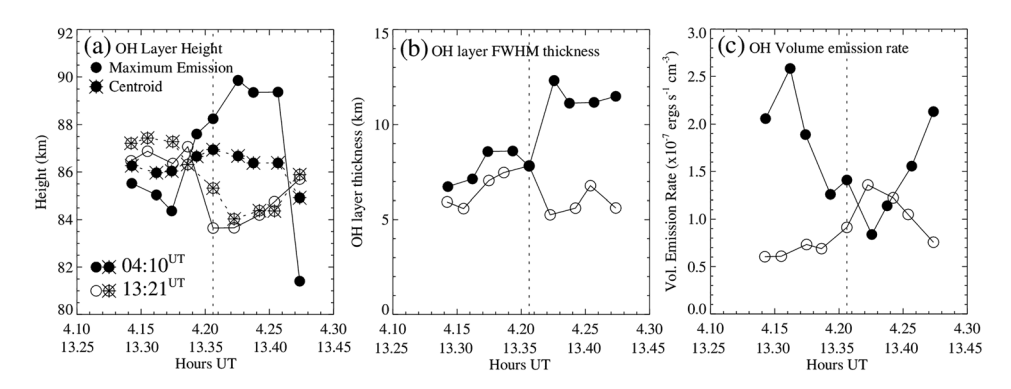
SABER instrument yielded MLT OH emission profiles and neutral temperature profiles. The first overpass occurred during the time of the wave event and was directed northward. The closest approach was 1,040 km at 04:12:22 UT. The second occurred over  $3\frac{1}{2}$  hr after observations ended for the night and was directed southward. The closest approach was 295 km at 13:20:47 UT. The ground tracks and the nine closest measurement locations from each overpass are shown in Figure 3.

Figure 4 shows the OH emission and temperature profiles obtained by SABER during the first overpass of El Leoncito. For clarity, only five of the nine analyzed profiles are shown here. At 04:12 UT, at closest approach, the altitude of maximum OH emission occurred at 88.3 km and the layer exhibited a vertical thickness as



**Figure 4.** Composite (a) OH emission profiles and (b) neutral MLT temperatures during the first SABER overpass. The solid black profiles (marked with an asterisk \*) were obtained at closest approach (04:12:22 UT). The distortion of the profiles by the gravity waves is clearly evident.

SMITH ET AL. 4 of 12



**Figure 5.** Derived OH layer parameters from SABER measurements during the two overpass periods: 04:12 UT (filled circles) and 13:21 UT (open circles). (a) Height of maximum OH emission and centroid height, (b) FWHM layer thickness, and (c) peak volume emission rate. The vertical dotted line corresponds to the time of closest approach to El Leoncito.

defined as the full-width at half-maximum emission (FWHM) of 7.8 km (Figure 4a). The mean centroid altitude was 86.9 km. The centroid height is defined as the central height of the FWHM thickness of the emission layer.

All of the profiles exhibited behavior that was consistent with the passage of a gravity wave, particularly the later profiles. After 04:12 UT, the profiles exhibited large variations in altitude and profile shape. Of the nine profiles, seven exhibited double peaked structures, indicating that gravity wave activity was distorting the profiles significantly. The distortion was also evident from the (~2–3 km) differences in the altitudes of the emission maximum and centroid of the OH emission (Figure 4a).

Similarly, in Figure 4b, large variations in the temperature profiles (of 40–50 K) also occurred over altitudes of 2–3 km. FFT analysis of the SABER profiles indicated the presence of gravity wave activity exhibiting a vertical wavelength of  $\lambda_z=11.5\pm4.2$  km, which is consist with the results determined earlier from the wave analysis of all-sky images.

Figure 5 shows several OH emission layer parameters derived from the SABER measurements during the two overpass periods; height of maximum emission, centroid height, layer FWHM thickness, and the peak volume emission rate.

During the first overpass, as SABER traveled northward and began sampling the region occupied by the propagating gravity waves, the altitude of maximum OH emission increased from near 84 to 90 km (Figure 5a). An even larger decrease, from 89 to 81 km, can also be seen to occur near the end of the first overpass. The centroid altitude of the OH emission remained at a relative constant altitude of 86–87 km.

The reason for the differences observed between the emission maximum and centroid heights can be explained as follows. One effect of gravity wave propagation through an emission layer is to cause an increase or decrease in the altitude of the emission profile. Wave disturbances with a vertical wavelength comparable to the layer thickness will also cause the profile to distort and possibly create double emission maxima. Hence, the height of maximum OH emission is particularly sensitive to such wave disturbances. In contrast, the centroid height, being the height of the layer as a whole, is less sensitive to such disturbances and distortions, for a given disturbance.

During the second overpass (13:21 UT), a similar but smaller decrease in OH height also occurred, from 88 to 83 km. The centroid altitude values were also more in agreement with the corresponding maximum emission altitudes, which indicated that the layer was subject to altitude variations by a much larger-scale disturbance and not the smaller-scale waves from during the earlier overpass.

The OH layer also exhibited significant variations in vertical thickness as a result of the gravity wave event. In Figure 5b, the FWHM thickness of the OH emission layer exhibited a large and sudden increase of 4.5 km (58%), from 7.8 km to 12.3 km (Figure 5b). Again, the abrupt changes exhibited by the OH emission can be explained by the passage of the gravity wave disturbance.

SMITH ET AL. 5 of 12

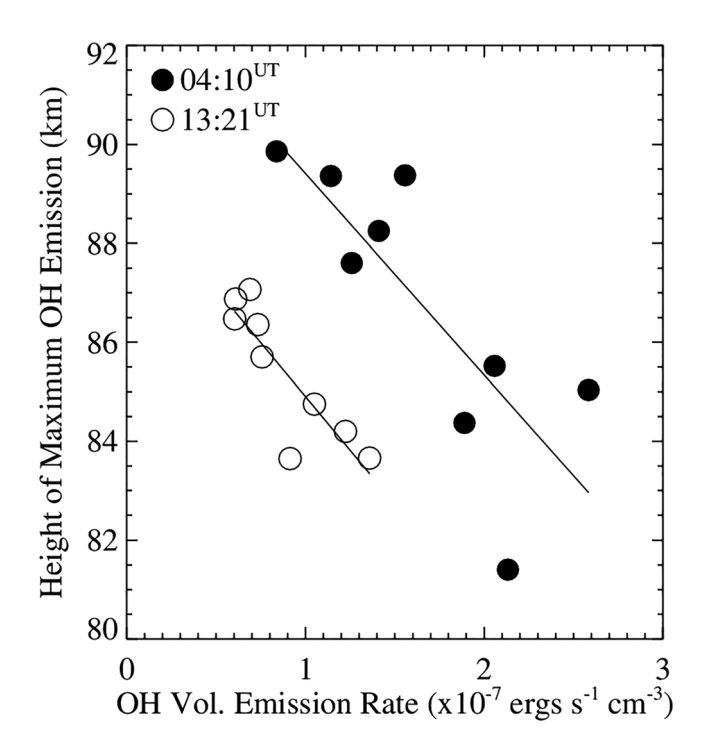


**Figure 6.** Plot of the height of maximum OH emission and the OH peak volume emission rate derived from SABER observations over the El Leoncito Obs. on the night of 18 March 2016. A strong relationship is observed due to the sensitivity of the OH VER to temperature.

The OH layer also exhibited substantial variations in emission rate, particularly during the first overpass. As can be seen in Figure 5c, the peak volume emission rate (VER) decreased by 68%, along the trajectory, in less than 4 min. The OH VER was more stable during the second overpass period, suggesting less gravity wave activity. The OH VER is sensitive to temperature. The observed variations were consistent with corresponding changes in the layer height, as shown in Figure 6.

The TIMED satellite traveled southward and approached closer to El Leoncito, during the second overpass period. Overall, the corresponding wave parameters, as shown in Figure 5, exhibited much less variation than during the first overpass, which suggests that the thunderstorm and its activity had diminished significantly.

#### 3.3. Meteosat-10 Satellite Imaging

The EUMETSAT geostationary weather satellite Meteosat-10 obtains full-Earth images with a 15-min cadence. Figure 7 is a time sequence of infrared images obtained by Metosat-10 at 90-min intervals during the night of 18 March 2016. A mesoscale thunderstorm complex can be seen to extend over the eastern region of Argentina, slowly evolving eastward and then northward over the course of the night. The Meteosat-10 images show that the thunderstorm began to develop over southeastern Argentina 18–19 UT on 16 March and slowly evolved northwestward over the following hours. The location of the system is consistent with it being the source of the gravity waves observed at El Leoncito. It is evident from Figure 7 that there were multiple centers of thunderstorm activity occurring simultaneously and so multiple epicenters of wave activity.

# 3.4. Suomi-NPP Day/Night Band Observation

Another instrument capable of observing gravity waves in nightglow is the Visible Infrared Imaging Radiometer Suite (VIIRS) onboard the Suomi-NPP satellite (Miller et al., 2015). The satellite overflew the El Leoncito region at ~05:15 UT on the night of 18 March, 2016 and obtained an image of the gravity wave field together with the thunderstorm complex. Figure 8 is a blended sandwich product image (Setvák et al., 2013) obtained at 05:18 UT from the VIIRS instrument using the day-night (DNB) and M15 IR-window bands. The image time was approximately halfway between the images times of Figures 7c and 7d.

This is also a unique case of an observation of gravity waves in nightglow, registered while the Moon was still above the local horizon, illuminating the storm tops. The DNB is a panchromatic band spanning the visible region from 500 to 900 nm. It therefore includes all three mesospheric emissions recorded by the El Leoncito imager— $O(^1S)$ , Na, and OH emissions, and so the wave patterns shown in Figure 8 are a blend of all three. The M15 IR-window band color enhancement ranges from 240 (blue) to 190 K (dark red). The combination of the two bands enables easy tracking of sources of various gravity waves and also provides information on storm top morphology.

The low emissivity of nightglow usually requires dark, moonless conditions in order for the VIIRS instrument to record gravity waves. The case described in this paper is the only one known to the authors in which gravity waves were recorded in moonlight—the Moon was at  $\sim 6^{\circ}$  above local horizon, 35 min before moonset, and 5 days before full. Despite these unfavorable conditions, the gravity waves are clearly visible—a further indication of the exceptional brightness of this event.

Well-developed gravity waves, in a form of concentric gravity waves (CGW's), can be seen northwest of the westernmost storm cell. This storm exhibits several storm top features typical for severe storms—distinct cold ring, overshooting top, cloud top concentric gravity waves, radial cirrus, and a well-developed above anvil cirrus plume, and so the storm was very likely to produce strong updrafts, generating the upward propagating gravity waves. While the storm tops are near the tropopause level or slightly above it, the CGW's observed in the nightglow are much higher, near the mesopause, as described elsewhere in the paper.

SMITH ET AL. 6 of 12

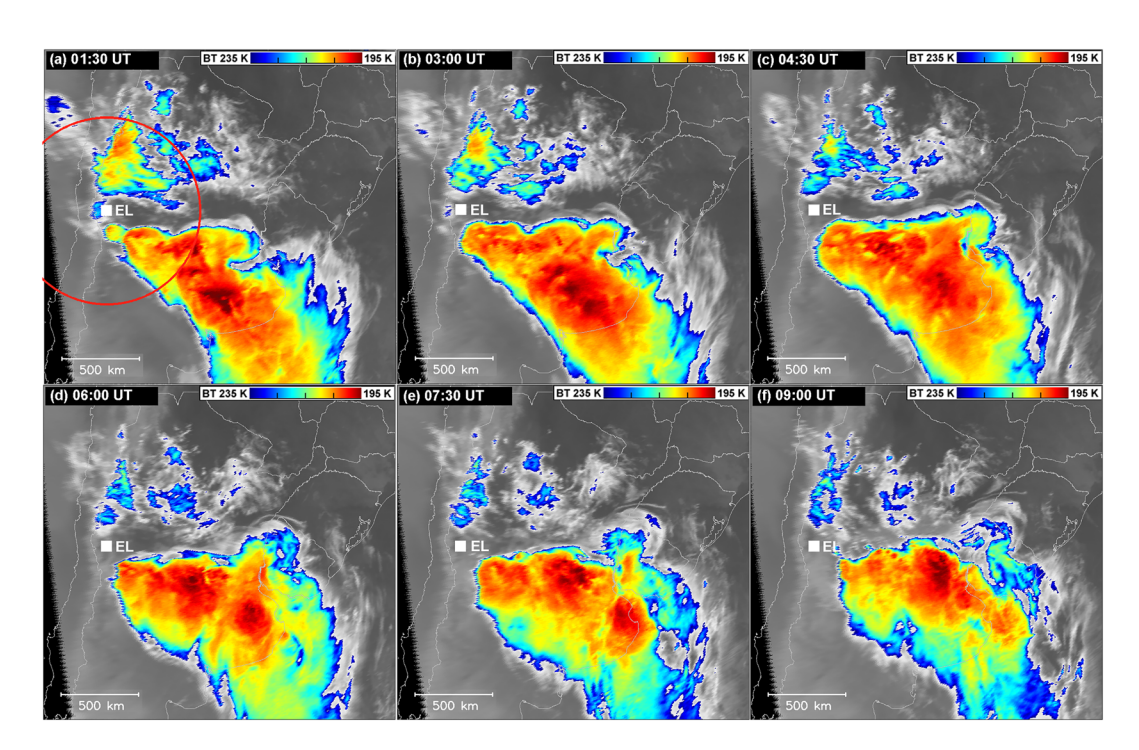


**Figure 7.** (a-f) Sequence of color-enhanced infrared satellite images (SEVIRI band IR10.8) over South America by the EUMETSAT Meteosat-10 during 01:30–09:00 UT on 18 March 2016. A mesoscale thunderstorm complex over Argentina is clearly evident. The storm system lay to the southeast of the El Leoncito Obs. ("EL") and gradually moved eastward over the course of the night. The all-sky imager's field of view is shown as a red circle.

The location of the storms and CGW's shown in Figure 8 are close to the nadir of the satellite and so parallax shifts can be neglected. The red dot indicates location of the El Leoncito Observatory. The horizontal wavelength of the waves exhibited in the nightglow near El Leoncito was  $\sim$ 35 km. Given the passage time of gravity waves from storm tops to the upper mesosphere ( $\sim$ 114 min), it is likely that these waves were generated by earlier activity from this storm, or its precursors at the same location. The smaller-scale, irregular gravity

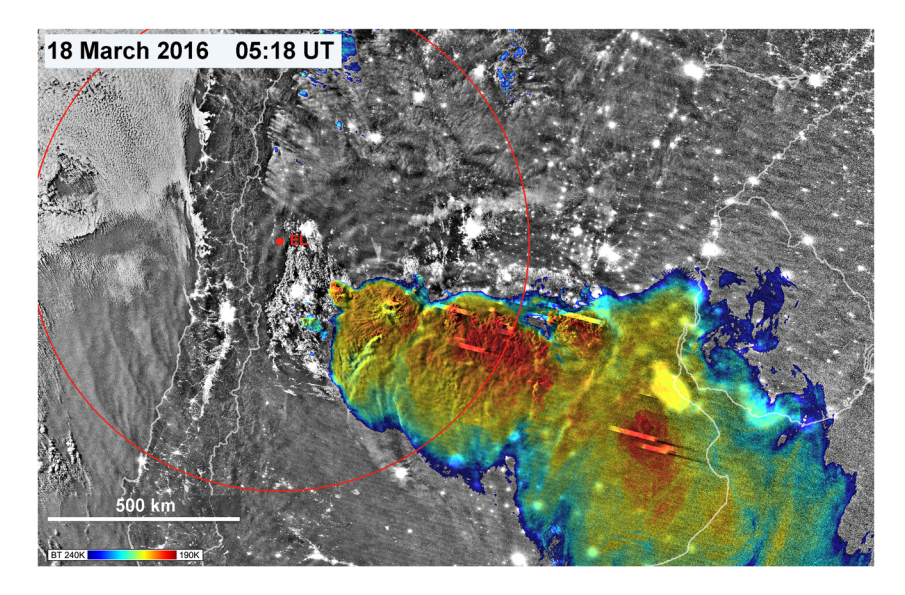


**Figure 8.** Composite sandwich image from the Suomi-NNP satellite on 18 March 2016 at 05:18 UT using the VIIRS day/night and the color-enhanced M15 bands. The all-sky field of view at the El Leoncito Observatory (red dot) is marked as the large red circle.

SMITH ET AL. 7 of 12

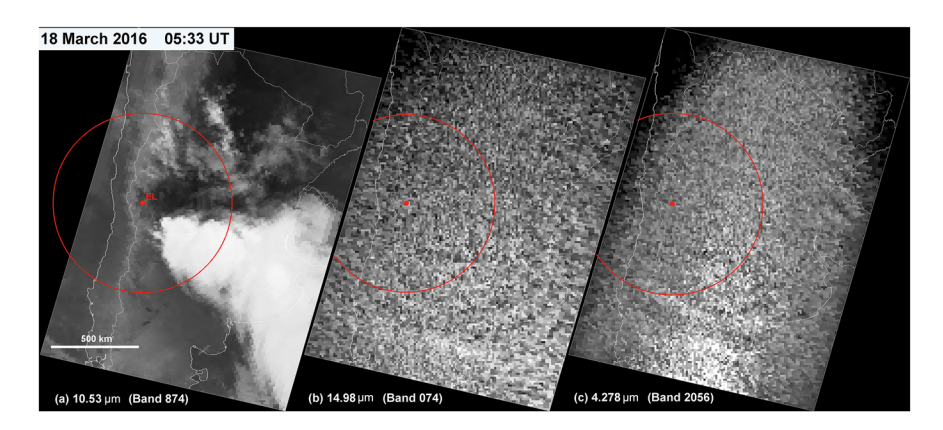


**Figure 9.** AIRS images on 18 March 2016 at 05:33 UT showing the (a) thunderstorm system and clouds over Argentina at 10.5  $\mu$ m and concentric stratospheric gravity waves at 30–40 km altitude at (b) 15.0 and (c) 4.3  $\mu$ m. The all-sky field of view at the El Leoncito Observatory (red dot) is marked as the large red circle.

waves to the northeast of the system appear to be a result of superposition of gravity waves generated by several sources (storm cells) within the system.

#### 3.5. NASA Aqua Satellite: AIRS Observations

The NASA Aqua satellite overflew El Leoncito on 18 March 2016 at 05:33 UT, ~15 min after Suomi, documenting the area with the onboard Atmospheric Infrared Sounder (AIRS), a 2,378-band hyperspectral grating spectrometer. The AIRS records, among others, the  $\rm CO_2$  fundamental bands at 4.3 and 15.0  $\mu$ m, which can be used to detect gravity wave-induced temperature variations from the 30–40 km altitude region in the upper stratosphere (Figure 9).

Figure 9a presents the context of the thunderstorm morphology over Argentina in the 10.53- $\mu$ m band. Figures 9b and 9c are the brightness temperature perturbation fields at 15.0 and 4.3  $\mu$ m, respectively.

Both fields exhibit large-scale concentric stratospheric gravity waves with a mean  $\lambda_x=160$  km ( $\sigma=35$  km), much larger than exhibited in the all-sky images. Due to the weighting functions used, AIRS detects larger-scale wave perturbations ( $\lambda_x>15$ –20 km,  $\lambda_z>40$ –50 km) compared to the ASI ( $\lambda_x>1$ –2 km,  $\lambda_z>6$ –8 km). Hence, the imagers can detect the smaller-scale gravity waves, which tend to exhibit larger momentum fluxes compared to the larger-scale waves.

By using the SABER temperature profile from 04:12:22 UT, and deriving  $\tau_b$  averaged over 30- to 88-km altitude region ( $\tau_b = 5.2$  mins), we can estimate the time taken to reach the mesospheric OH layer. If we assume  $\lambda_z = 40$ –50 km for the gravity waves in Figure 9c (near the lower end of the vertical resolution of AIRS), we can use

$$C_{gz} = -\frac{Nkm}{\left(k^2 + m^2 + \frac{1}{4H^2}\right)^{3/2}} \tag{1}$$

(Fritts & Alexander, 2003), which yields  $c_{\rm gz}=20.6\pm7.9~{\rm m~s^{-1}}$  with a travel time from 35 km to the OH layer of 43  $\pm$  16 min ( $\lambda_z=40~{\rm km}$ ). For  $\lambda_z=50~{\rm km}$ :  $c_{\rm gz}=26.3\pm10.0~{\rm m~s^{-1}}$  with a travel time of 34  $\pm$  13 min. These estimates are markedly different from the earlier estimates obtained via the all-sky wave parameters, which suggests that the two systems are recording different scale sizes associated with the same disturbance.

The wave patterns in Figures 9b and 9c are strongest to the south and northeast of El Leoncito but are weak over the site, probably due to the presence of moonlight in the northwestern sky. The centers of the patterns also correspond closely with the location of the main convection center shown in Figure 8 (and Figure 7), near the edge of the field of view of the ASI, which further supports a thunderstorm origin for the mesospheric waves.

SMITH ET AL. 8 of 12

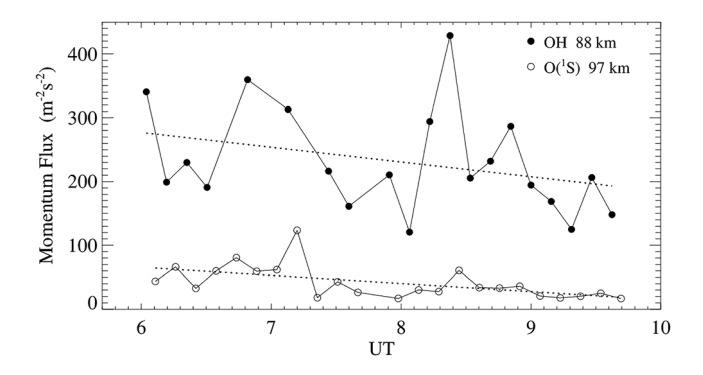


**Figure 10.** Measured vertical flux of horizontal momentum over the El leoncito Observatory during the night of 18 March 2016.

# 4. Results and Discussion

# 4.1. Gravity Wave Momentum Flux

The vertical flux of horizontal momentum (per unit mass),  $F_m$ , associated with the gravity wave was derived using the relation (Swenson & Liu, 1998; Vargas et al., 2007):

$$F_{m} = -\frac{1}{2} \frac{g^{2}}{N^{2}} \frac{\lambda_{z}}{\lambda_{x}} \left(\frac{I'}{I_{m}}\right)^{2} \frac{1}{CF^{2}} = -46.85 \frac{1}{N^{2}} \frac{\lambda_{z}}{\lambda_{x}} \left(\frac{I'}{I_{m}}\right)^{2} \frac{1}{CF^{2}}$$
(2)

where g is the acceleration due to gravity (= 9.68 m s<sup>-2</sup> at 88-km altitude), N is the Brunt-Vaisala frequency derived from the SABER temperature profile, I' is the measured airglow mean-to-peak wave amplitude,  $I_m$  is the mean measured airglow brightness, and CF is the cancellation factor

(described next). The method utilizes the measured airglow brightness amplitude (mean-to-peak) to infer the gravity wave temperature perturbation amplitude and estimate the momentum flux.

The Brunt-Vaisala frequency was derived from the closest SABER temperature profile (04:12:22 UT) using the mean value of  $N^2$  calculated using derived values within FHWM/2 of the altitude of the maximum airglow emission as determined by the SABER—88.2 km for OH and 97 km for O( $^1$ S).

The all-sky imaging technique records the integrated brightness through an emission layer of finite width and so the cancellation factor, CF, models the effect of phase averaging or cancellation of the wave due to the finite thickness of the layer. The airglow modulation due to gravity waves with vertical scale sizes comparable to the layer width will be weakened compared to waves with much larger  $\lambda_z$ . The cancellation factor has the following form:

$$CF = c_0 - c_1 \exp\left[-c_2(\lambda_z - 6 \text{ km})^2\right]$$
(3)

where  $c_0$ ,  $c_1$ , and  $c_2$  are constants (Vargas et al., 2009).

Figure 10 shows the measured vertical flux of horizontal momentum flux associated with the OH and O( $^1$ S) gravity waves during the night from 06:00 to 10:00 UT. The estimates were deduced from individual images in order to investigate the variation in the momentum flux during the course of the night, instead of estimating the flux for the entire event or night, as done previously. The momentum flux values for the OH emission decreased from ~300 to ~150 m² s<sup>-2</sup> during that time with a mean value of  $F_m = 232$  m² s<sup>-2</sup> ( $\sigma = 82$  m² s<sup>-2</sup>). The O( $^1$ S) emission also decreased during the night from ~60 to ~30 m² s<sup>-2</sup> with a mean value of  $F_m = 42$  m² s<sup>-2</sup> ( $\sigma = 26$  m² s<sup>-2</sup>).

Notably, the momentum flux values were several times larger than those typically observed in mesospheric gravity wave events  $(1-15~\text{m}^2~\text{s}^{-2})$  (e.g., Swenson et al., 1999; Tang et al., 2014; Vargas et al., 2009). The OH flux values were an order of magnitude larger than typical and over five times larger than the  $O(^1S)$  values, which suggests that a large amount of wave energy was dissipated in the altitude region between the two emission layers. The SABER temperature profiles exhibited relatively large inversion features of 15–45 K above the OH layer at 88 km (Figure 4), which is suggestive of turbulent dissipation heating, although there is no evidence of wave breaking or small-scale instabilities in the images. No wind information was available during the night, so any effects involving possible wave-wind interactions could not be ascertained.

Both emissions exhibited a decrease in wave amplitude (not shown) and momentum flux during the night (Figure 10), possibly due to temporal evolution of the underlying thunderstorm or by variations within the intervening stratosphere and lower mesosphere. Most importantly, the large momentum flux values exhibited by the wave event indicate that thunderstorm systems can generate gravity waves that are able to transport significant amounts of momentum flux routinely into the upper atmosphere/ionosphere.

In this study, momentum flux is determined by an indirect estimate of the temperature perturbation ratio  $(T'/T_m)$  due to the gravity wave by using airglow  $(I'/I_m)$  measurements via CF. The airglow brightness is dependent upon several variables such as the photochemistry, temperature, and number density, which can contribute to uncertainties in the momentum flux values. The derived momentum flux values are

SMITH ET AL. 9 of 12



very sensitive to the airglow brightness perturbation amplitude, I', and to  $\lambda_z$ , especially when  $\lambda_z \sim$  FWHM of the layer. As a result, these two parameters contribute significantly to the uncertainties in the momentum flux, which, in some cases, can be 50–70% or more. Despite its limitations, the all-sky imaging method can provide momentum flux estimates on timescales of minutes, over a large horizontal extent.

In general, all-sky multispectral imaging can record smaller-scale sizes with higher sensitivity and over longer timescales compared to satellite systems. An imaging system can record wave activity on time-scales of minutes over the course of several hours, whereas a satellite may make perhaps only one or two passes per day over the same region. Furthermore, the smaller-scale scales recorded by ASIs tend to be those that exhibit large momentum and energy fluxes and thus are important to mesospheric and thermospheric dynamics.

### 4.2. Maximum Altitude of Gravity Wave Propagation

If the O( $^1$ S) gravity waves did not exhibit any obvious signs of breaking or instability and continued to propagate to higher altitudes unobserved, how high would they have reached before breaking or dissipating? Gravity wave propagation may occur when the vertical phase speed of the wave ( $\omega/m$ ) is higher than the vertical velocity of diffusion (mD), where the vertical wavenumber  $m = 2\pi/\lambda_z$  and D is the effective molecular diffusion coefficient (Gardner, 1994; Gossard & Hooke, 1975). Above 100 km, diffusion processes become increasingly important and, as a result, wave damping will occur. For a gravity wave of  $\lambda_z$ , the damping limit  $D_{\text{max}}$  occurs when  $D = \omega/m^2 = \lambda_z^2/2\pi T_{\text{int}}$ , where  $T_{\text{int}}$  is the intrinsic gravity wave period.

Values for D were derived from [O],  $[O_2]$ ,  $[N_2]$ , and temperature profiles using the NRLMSISE-00 atmospheric model (Picone et al., 2002) and using the wave parameters obtained from the OH and  $O(^1S)$  images. From this analysis, we estimate the propagation altitude limit for this wave event to be 120–125 km, which is consistent with the results of Swenson et al. (1995) who also used all-sky imaging data.

### 5. Summary

The Boston University ASI at the El Leoncito Observatory recorded a large and bright gravity wave event in the three mesospheric emissions of OH, Na, and O( $^1$ S). All-sky imaging data evidence indicates that the source of the waves was a large thunderstorm complex located southeast of El Leoncito. In addition, NASA Aqua and NASA/National Oceanic and Atmospheric Administration (NOAA) Suomi-NNP satellite images indicate concentric gravity wave activity associated with the complex at two distinct altitude regions—in the stratosphere near 30–40 km and the mesosphere at 85–100 km. Thunderstorms have long been known to be a source of mesospheric waves but this event was remarkable for its brightness and longevity.

The vertical flux of horizontal momentum associated with the gravity waves was derived from the all-sky data and thus yielded a high time resolution measure of the activity associated with the thunderstorm, and its evolution during the course of the night. The values also provided a measure of the evolution of the effects of the thunderstorm on the mesosphere. Most importantly, the momentum fluxes associated with the waves were significantly larger than exhibited in mesospheric gravity wave events typically.

The maximum altitude reached by the wave event was estimated from the dispersion equation and molecular diffusion arguments to be near 120–125 km in the lower thermosphere.

The precise role of gravity waves in the variability of the mesosphere and thermosphere/ionosphere is still largely unknown. Large differences exist, both geographically and seasonally. Small-scale short-period gravity waves, that is, those typically recorded by ASIs, are known to transport considerable amounts of wave momentum into the region and to contribute significantly to the region's dynamics and variability, which is important consideration for an accurate census of the momentum flux associated with wave events. In addition, ASIs can provide essentially continuous momentum flux estimates throughout the night, whereas satellite measurements tend to be limited to perhaps one or two measurements per night in the region of the station.

The gravity wave event presented here illustrates the importance of thunderstorm activity as one contribution to wave energy and momentum transport from below and how such events play a role in quantifying that variability and increasing our understanding of space weather dynamics.

SMITH ET AL. 10 of 12



# **Data Availability Statement**

The data used in this study are available at the following:

- Boston University all-sky data (http://sirius.bu.edu/dataview/). The data are presented as a clickable calendar listing.
- 2. TIMED SABER Data (http://saber.gats-inc.com/browse\_data.php).
- 3. Click "V2.0" then "Level 2A," then "2016," then "MAR," and then "18."
- 4. Meteosat-10 SEVIRI (HRIT) data: EUMETSAT Data Archive (https://eoportal.eumetsat.int/).
- Suomi-NPP VIIRS (L1B) data: NOAA CLASS archive (https://ladsweb.modaps.eosdis.nasa.gov/missions-and-measurements/products/VNP02IMG/).
- 6. Aqua AIRS (AIRIBRAD) data: NASA GESDISC Data Archive (https://airsl1.gesdisc.eosdis.nasa.gov/data/Aqua\_AIRS\_Level1/AIRIBRAD.005/).

#### Acknowledgments

This work was funded by an award from the Office of Naval Research (N00014-20-1-2068) [S. M. S]. Part of this work was supported by the Czech Ministry of Environment, DKRVO, CHMI 2018-2022 program [M. S.]. We are grateful to the director and staff at CASLEO for their continued support of our research efforts at El Leoncito. We are grateful to S. C. Smith for helpful discussions and continued support [S. M. S.]. We also wish to thank the two reviewers of this manuscript for their useful comments and suggestions.

#### References

Armstrong, E. B. (1982). The association of visible airglow features with a gravity wave. *Journal of Atmospheric and Terrestrial Physics*, 44, 325–336. https://doi.org/10.1016/0021-9169(82)90077-0

Barnard, E. E. (1911). Self-luminous night haze. Proceedings of the American Philosophical Society, 50(199), 246-253.

Bates, D. R. (1960). Bright nights. In J. A. Ratcliffe (Ed.), *Physics of the upper atmosphere* (pp. 236–237). San Diego, CA: Academic Press. Baumgardner, J., Flynn, B., & Mendillo, M. (1993). Monochromatic imaging instrumentation for applications in aeronomy of the Earth and planets. *Optical Engineering*, 32(12), 3028–3032. https://doi.org/10.1117/12.149194

Baumgardner, J., Wroten, J., Semeter, J., Kozyra, J., Buonsanto, M., Erickson, P., & Mendillo, M. (2007). A very bright SAR arc: implications for extreme magnetosphere-ionosphere coupling. *Annales Geophysicae*, 25, 2593–2608.

Dewan, E. M., Picard, R. H., O'Neil, R. R., Gatdiner, H. A., Gibson, J., Mill, J. D., et al. (1998). MSX satellite observations of thunderstorm-generated gravity waves in mid-wave infrared images of the upper stratosphere. *Geophysical Research Letters*, 25, 939–942. https://doi.org/10.1029/98GL00640

Fritts, D. C., & Alexander, M. J. (2003). Gravity wave dynamics and effects in the middle atmosphere. *Reviews of Geophysics*, 41(1), 1003. https://doi.org/10.1029/2001RG000106

Gardner, C. S. (1994). Diffusive filtering theory of gravity wave spectra in the atmosphere. *Journal of Geophysical Research*, 99(D10), 20601. https://doi.org/10.1029/94JD00819

Gledhill, J. (1874). Aurora? (Vol. 12, p. 196). London: Astron. Register, Roy. Astron. Soc.

Gossard, E. E., & Hooke, W. H. (1975). Waves in the atmosphere: Atmospheric infrasound and gravity waves - Their generation and propagation, Developments in Atmospheric Science, 2 (470 pp.). Amsterdam: Elsevier.

Herse, M. (1988). Bright nights. In W. Schroeder (Ed.), Past, present and future trends in geosciences (pp. 40–64). Bremen-Roennebeck: IAGA Interd. Comm. History.

Hoffmeister, C. (1951). Ergebnisse Der Exakten Naturwissenschaften (Vol. 24, pp. 1-53). Berlin: Springer-Verlag.

Hoffmeister, C. (1952). Investigation on the bright night sky and luminous bands. British Astronomical Association, 62(8), 288-292.

Hoffmeister, C. (1960). Interplanetare Materie und Verstärktes Nachthimmelleuchten. In Zeitschrift für Astrophysik (Vol. 49, pp. 233–242). Berlin.

Martinis, C. R., Baumgardner, J., Smith, S. M., Colerico, M., & Mendillo, M. (2006). Imaging science at El Leoncito, Argentina. *Annales de Geophysique*, 24, 1–12. https://doi.org/10.5194/angeo-24-1375-2006

Martinis, C. R., Baumgardner, J., Wroten, J., & Mendillo, M. (2017). All-sky-imaging capabilities for ionospheric space weather research using geomagnetic conjugate point observing sites. *Advance Space Physics*, 61(7), 1636–1651. https://doi.org/10.1016/j.

Miller, S. D., Straka, W. C. I. I. I., Yue, J., Smith, S. M., Alexander, J., Hoffmann, L., et al. (2015). Upper atmospheric gravity wave details revealed in nightglow satellite imagery. PNAS 2015, 112(49), E6728–E6735. https://doi.org/10.1073/pnas.1508084112

Peterson, A. (1979). Airglow events visible to the naked eye. Applied Optics, 18, 3390-3393. https://doi.org/10.1364/AO.18.003390

Picard, R. H., O'Neil, R. R., Gardiner, H. A., Gibson, J., Winick, J. R., Gallery, W. O., et al. (1998). Remote sensing of discrete stratospheric gravity-wave structure at 4.3μm from the MSX satellite. *Geophysical Research Letters*, 25(15), 2809–2812. https://doi.org/10.1029/98gl01701

Picone, J. M., Hedin, A. E., Drob, D. P., & Aikin, A. C. (2002). NRLMSISE-00 empirical model of the atmosphere: Statistical comparisons and scientific issues. *Journal of Geophysical Research*, 107(A12), 1468P. https://doi.org/10.1029/2002JA009430

Rayleigh, L. (1931). On a night sky of exceptional brightness, and on the distinction between the polar aurora and the night sky. *Proceedings of the Royal Society of London, Series A*, 131(817), 376–381.

Sentman, D. D., Wescott, E. M., Picard, R. H., Winick, J. R., Stenbaek-Nielsen, H. C., Dewan, E. M., et al. (2003). Simultaneous observations of mesospheric gravity waves and sprites generated by a Midwestern thunderstorm. *Journal of Atmospheric and Solar - Terrestrial Physics*, 65, 537–550. https://doi.org/10.1016/S1364-6826(02)00328-0

Setvák, M., Bedka, K., Lindsey, D. T., Sokol, A., Charvát, Z., Šťástka, J., & Wang, P. K. (2013). A-Train observations of deep convective storm tops. Atmospheric Research, 123, 229–248. https://doi.org/10.1016/j.atmosres.2012.06.020

Shepherd, G. G., & Cho, Y.-M. (2017). WINDII airglow observations of wave superposition and the possible association with historical "bright nights". *Geophysical Research Letters*, 44, 7036–7043. https://doi.org/10.1002/2017GL074014

Skey, H. (1902). Notes on the Aurora in the Southern Hemisphere. In *Trans. and Proc. Roy. Soc. of N.Z.* (Vol. 35, pp. 405–408). Wellington. Smith, S. M., Baumgardner, J., & Mendillo, M. (2009). Evidence of mesospheric gravity-waves generated by orographic forcing in the troposphere. *Geophysical Research Letters*, 36, L08807. https://doi.org/10.1029/2008GL036936

Smith, S. M., Martinis, C. R., Baumgardner, J., & Mendillo, M. (2015). All-sky imaging of transglobal thermospheric gravity waves generated by the March 2011 Tohoku Earthquake. *Journal of Geophysical Research: Space Physics*, 120, 10,992–10,999. https://doi.org/10.1002/2015JA021638

SMITH ET AL. 11 of 12



- Smith, S. M., Scheer, J., Reisin, E., Baumgardner, J., & Mendillo, M. (2006). Characterization of two exceptionally strong mesospheric wave events observed at El Leoncito, Argentina, using all-sky and zenith airglow observations. *Journal of Geophysical Research*, 111, A09309. https://doi.org/10.1029/2005JA011197
- Smith, S. M., Taylor, M. J., Swenson, G. R., She, C.-Y., Hocking, W., Baumgardner, J., & Mendillo, M. (2003). A multidiagnostic investigation of the mesospheric bore phenomenon. *Journal of Geophysical Research*, 108(A2), 1083. https://doi.org/10.1029/2002JA009500
- Swenson, G. R., Gardner, C. S., & Taylor, M. J. (1995). Maximum altitude penetration of atmospheric gravity waves observed during the ALOHA-93. Geophysical Research Letters. 22(20), 2857–2860.
- Swenson, G. R., Haque, R., Yang, W., & Gardner, C. S. (1999). Momentum and energy fluxes of monochromatic gravity waves observed by an OH imager at Starfire Optical Range, New Mexico. *Journal of Geophysical Research*, 104(D6), 6067–6080. https://doi.org/10.1029/1998JD200080
- Swenson, G. R., & Liu, A. Z. (1998). A model for calculating acoustic gravity wave energy and momentum flux in the mesosphere from OH airglow. *Geophysical Research Letters*, 25, 477–480. https://doi.org/10.1029/98GL00132
- Tang, Y., Dou, X., Li, T., Nakamura, T., Xue, X., Huang, C., et al. (2014). Gravity wave characteristics in the mesopause region revealed from OH airglow imager observations over Northern Colorado. *Journal of Geophysical Research: Space Physics*, 119, 630–645. https://doi.org/ 10.1002/2013JA018955
- Taylor, M. J., & Hapgood, M. A. (1988). Identification of a thunderstorm as source of short period gravity waves in the upper atmospheric nightglow emissions. *Planetary and Space Science*, 36(10), 975–985. https://doi.org/10.1016/0032-0633(88)90035-9
- Taylor, M. J., Hapgood, M. A., & Rothwell, P. (1987). Observations of gravity wave propagation in the OI(557.7 nm), Na (589.2 nm) and the near infra-red OH nightglow emissions. *Planetary and Space Science*, 35, 413–427. https://doi.org/10.1016/0032-0633(87)90098-5
- Taylor, M. J., Turnbill, D. N., & Lowe, R. P. (1995). Spectrometric and imaging measurements of a spectacular gravity wave event observed during the ALOHA-93 campaign. *Geophysical Research Letters*, 22, 2849–2852. https://doi.org/10.1029/95GL02948
- Vadas, S. L., Taylor, M. J., Pautet, P.-D., Stamus, P. A., Fritts, D. C, Liu, H.-L., et al. (2009). Convection: The likely source of medium-scale gravity waves observed in the OH airglow layer near Brasilia, Brazil, during the SpreadFEx Campaign. *Annales Geophysicae*, 27, 231–259. https://doi.org/10.5194/angeo-27-231-2009
- Vadas, S., Yue, J., & Nakamura, T. (2012). Mesospheric concentric gravity waves generated by multiple convective storms over the North American Great Plain. *Journal of Geophysical Research*, 117, D07113. https://doi.org/10.1029/2011JD017025
- Vargas, F., Gobbi, D., Takahashi, H., & Lima, L. M. (2009). Gravity wave amplitudes and momentum fluxes inferred from OH airglow intensities and meteor radar winds during SpreadFEx. Annales de Geophysique, 27, 2361–2369. https://doi.org/10.5194/angeo-27-2361-2009
- Vargas, F., Swenson, G., Liu, A., & Gobbi, D. (2007). O(1S), OH, and O<sub>2</sub>(b) airglow layer perturbations due to AGWs and their implied effects on the atmosphere. *Journal of Geophysical Research*, 112, D14102. https://doi.org/10.1029/2006JD007642
- Wu, D. L. (2004). Mesoscale gravity wave variances from AMSU-A radiances. Geophysical Research Letters, 31, L12114. https://doi.org/ 10.1029/2004GL019562
- Wu, D. L., & Eckermann, S. D. (2008). Global gravity wave variances from Aura MLS: Characteristics and Interpretation. Journal of the Atmospheric Sciences, 65, 3695–3718. https://doi.org/10.1175/2008JAS2489.1
- Wu, D. L., & Jiang, J. H. (2002). MLS observations of atmospheric gravity waves over Antarctica. *Journal of Geophysical Research*, 107(D24), 4773. https://doi.org/10.1029/2002JD002390
- Xu, J., Li, Q., Yue, J., Hoffmann, L., Straka, W. C. III, Wang, C., et al. (2015). Concentric gravity waves over northern China observed by an airglow imager network and satellites. *Journal of Geophysical Research: Atmospheres*, 120, 11,058–11,078. https://doi.org/10.1002/2015JD023786
- Xu, S., Yue, J., Xue, X., Vadas, S. L., Miller, S. D., Azeem, I., et al. (2019). Dynamical coupling between Hurricane Matthew and the middle to upper atmosphere via gravity waves. *Journal of Geophysical Research: Space Physics*, 124, 3589–3608. https://doi.org/10.1029/
- Yue, J., Hoffmann, L., & Alexander, M. J. (2013). Simultaneous observations of convective gravity waves from a ground-based airglow imager and the AIRS satellite experiment. *Journal of Geophysical Research: Atmospheres*, 118, 3178–3191. https://doi.org/10.1002/jord.50341
- Yue, J., Miller, S. D., Hoffmann, L., & Straka, W. C. III (2014). Stratospheric and mesospheric concentric gravity waves over tropical cyclone Mahasen: Joint AIRS and VIIRS satellite observations. *Journal of Atmospheric and Solar - Terrestrial Physics*, 119, 83–90. https://doi.org/ 10.1016/j.jastp.2014.07.003
- Yue, J., Vadas, S., She, C.-Y., Nakamura, T., Reising, S., Liu, H., et al. (2009). Concentric gravity waves in the mesosphere generated by deep convective plumes in the lower atmosphere near Fort Collins, Colorado. *Journal of Geophysical Research*, 114, D06104. https://doi.org/10.1029/2008JD011244

SMITH ET AL. 12 of 12